



# CHORUS

This is the accepted manuscript made available via CHORUS. The article has been published as:

## Measurement of prompt neutron polarization asymmetries in photofission of $^{235,238}\text{U}$ , $^{239}\text{Pu}$ , and $^{232}\text{Th}$

J. M. Mueller, M. W. Ahmed, B. Davis, J. M. Hall, S. S. Henshaw, M. S. Johnson, H. J. Karwowski, D. Markoff, L. S. Myers, B. A. Perdue, S. Stave, J. R. Tompkins, M. J. Tuffley, and H. R. Weller

Phys. Rev. C **85**, 014605 — Published 11 January 2012

DOI: [10.1103/PhysRevC.85.014605](https://doi.org/10.1103/PhysRevC.85.014605)

# A Measurement of Prompt Neutron Polarization Asymmetries in Photofission of $^{235,238}\text{U}$ , $^{239}\text{Pu}$ , and $^{232}\text{Th}$

J.M. Mueller,<sup>1,2</sup> M.W. Ahmed,<sup>1,2,3</sup> B. Davis,<sup>3</sup> J.M. Hall,<sup>4</sup> S.S. Henshaw,<sup>1,2,\*</sup>  
M.S. Johnson,<sup>4,5</sup> H.J. Karwowski,<sup>1,6</sup> D. Markoff,<sup>3</sup> L.S. Myers,<sup>1,2</sup> B.A.  
Perdue,<sup>1,2,†</sup> S. Stave,<sup>1,2,‡</sup> J.R. Tompkins,<sup>1,6</sup> M.J. Tuffley,<sup>5</sup> and H.R. Weller<sup>1,2</sup>

<sup>1</sup>*Triangle Universities Nuclear Laboratory, Durham NC 27708*

<sup>2</sup>*Department of Physics, Duke University, Durham NC 27708*

<sup>3</sup>*Department of Physics, North Carolina Central University, Durham NC 27707*

<sup>4</sup>*Lawrence Livermore National Laboratory, Livermore CA 94550*

<sup>5</sup>*Department of Physics and Astronomy,  
San Jose State University, San Jose CA 95192*

<sup>6</sup>*Department of Physics and Astronomy,  
University of North Carolina - Chapel Hill, Chapel Hill NC 27599*

(Dated: December 12, 2011)

## Abstract

A photofission experiment was performed on targets of  $^{235}\text{U}$ ,  $^{238}\text{U}$ ,  $^{239}\text{Pu}$ , and  $^{232}\text{Th}$  using nearly 100% linearly polarized, high intensity ( $\sim 10^7 \gamma/s$ ), and nearly-monoenergetic  $\gamma$ -ray beams having energies between 5.6 MeV and 7.3 MeV at the High Intensity  $\gamma$ -ray Source (HI $\gamma$ S). An array of 18 liquid scintillator detectors was used to measure prompt fission neutron polarization asymmetries. An asymmetry close to zero was found for  $^{235}\text{U}$  and  $^{239}\text{Pu}$  while a significant asymmetry ( $\sim 0.5$ ) was found for  $^{238}\text{U}$  and  $^{232}\text{Th}$ . A simplified model of near-threshold photofission has been developed in an attempt to explain the systematic difference between the even-even and even-odd targets. The results of a simulation, based on this model and using previous measurements of fission fragment angular distributions, are shown to accurately reproduce the essential features of the data.

---

\* Present location: National Security Technologies, Andrews Air Force Base MD 20762

† Present location: Los Alamos National Laboratory, Los Alamos NM 87544

‡ Present location: Pacific Northwest National Laboratory, Richland WA 99352

## I. INTRODUCTION

### A. Photofission Fragment Angular Distributions

The discovery of an anisotropy in photofission fragment angular distributions from  $^{232}\text{Th}$  in 1952 [1] prompted the development of the photofission channel formalism in 1956 [2]. This model relates the fragment angular distribution to the excitation spectrum of the highly deformed saddle-point nucleus. Each excited saddle-point state has a total angular momentum value  $J$  and an angular momentum projection along the symmetry axis  $K$ . The  $J$  and  $K$  quantum numbers specify the orientation of the deformed nucleus, which gives rise to the angular distribution of the fission fragments. For beam energies approaching the photofission threshold the saddle-point nucleus is assumed to be thermodynamically cold and only a few excited states are energetically accessible. If one of these states is more populated than the others or if the probability of penetrating the fission barrier is very different for these states, the resulting fragment angular distribution can become very anisotropic. For beam energies several MeV above the photofission threshold, more states are energetically available because the saddle-point nucleus is thermodynamically hot. When these states are equally populated and have similar barrier penetrabilities, the superposition of contributions from all of these individual states leads to an isotropic fragment angular distribution. This decrease in fragment anisotropy with increasing beam energy is qualitatively consistent with the experimental results of Ref. [1].

Since the pioneering work of Ref. [1], photofission fragment angular distributions have been measured for many other actinides and systematic differences have been observed between even-even and even-odd nuclei. Fragment angular distributions of several even-even targets have been measured to be very anisotropic near the photofission threshold [3], while photofission of several even-odd targets at similar beam energies yielded predominantly isotropic fragment angular distributions [4–7]. This systematic effect can be explained by differences in the nuclear spin and the excitation spectrum of the saddle-point nucleus. Because the even-odd nuclei have a randomly oriented nonzero spin, any observed anisotropy due to the absorption of a photon with spin 1 will be diminished relative to the case of an even-even nucleus with zero spin [8]. In addition to this effect, the level density near the photofission threshold of an even-odd saddle-point nucleus should be higher than for an

even-even saddle-point nucleus because the excitation spectrum at the saddle-point nucleus is expected to be similar to the ground state excitation spectrum [7]. Due to the higher number of fission channels in even-odd nuclei compared to even-even nuclei, the resulting fragment angular distribution should become more isotropic.

## B. Angular Distributions and Polarization Asymmetries in Photofission

Using the formalism in Ref. [9] and assuming only electric dipole and quadrupole photofission with no interference terms, the relative fragment or neutron yield as a function of polar angle ( $\theta$ ) can be parameterized as

$$W(\theta) = a + b \sin^2(\theta) + c \sin^2(2\theta), \quad (1)$$

Using these same assumptions, the angular distribution resulting from using a linearly polarized beam to induce fission can be obtained by using the prescription in Ref. [10]

$$W(\theta, \phi) = a + b \sin^2(\theta) + c \sin^2(2\theta) + P_\gamma \cos(2\phi)(b \sin^2(\theta) + c \sin^2(2\theta)). \quad (2)$$

where  $\phi$  is the azimuthal angle and  $P_\gamma$  is the beam polarization. Further simplification can be performed by neglecting the quadrupole contribution and assuming a 100% linearly polarized beam. Equation 2 then becomes

$$W(\theta, \phi) = a + b \sin^2(\theta) + b \cos(2\phi) \sin^2(\theta), \quad (3)$$

where  $a$  and  $b$  are normalized such that  $a + b = 1$ . Any dipole contribution to the anisotropy of the angular distribution, when using an unpolarized beam, leads to anisotropy in  $\phi$  when using a linearly polarized beam. Sensitivity of the measurement to  $b$  is increased with the use of a linearly polarized beam, as shown in Fig. 1.

The polarization asymmetry  $\Sigma(\theta)$  is given in terms of the neutron or fragment yields at different values of  $\phi$  by

$$\Sigma(\theta) = \frac{W(\theta, 0^\circ) + W(\theta, 180^\circ) - W(\theta, 90^\circ) - W(\theta, 270^\circ)}{W(\theta, 0^\circ) + W(\theta, 180^\circ) + W(\theta, 90^\circ) + W(\theta, 270^\circ)}. \quad (4)$$

Using Eqn. 3, this reduces to

$$\Sigma(\theta) = \frac{A \sin^2(\theta)}{1 + A \sin^2(\theta)}, \quad (5)$$

where  $A = b/a$ .

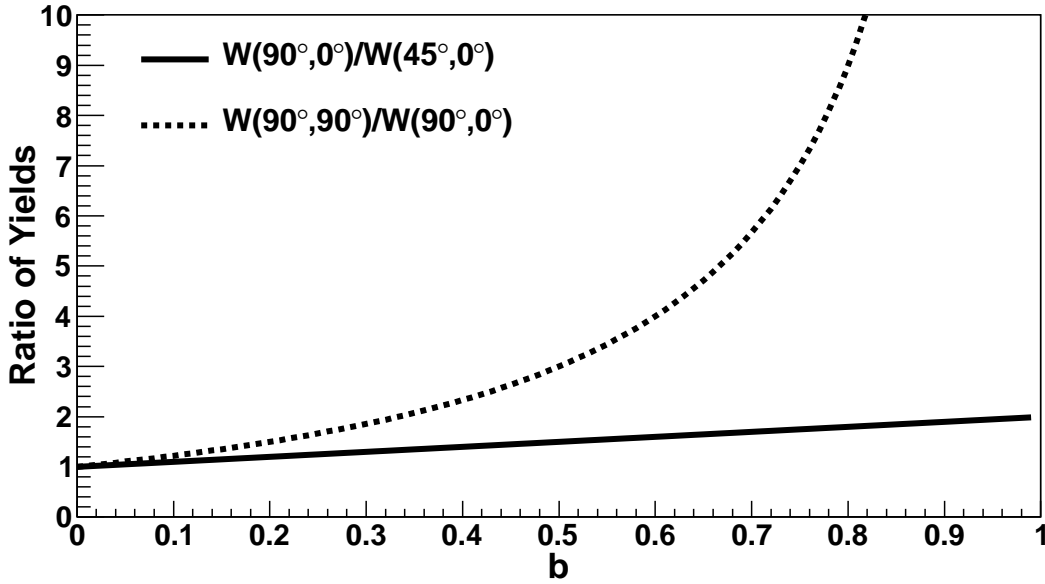


FIG. 1. The ratio of yields at  $\theta = 45^\circ$  and  $90^\circ$  for an unpolarized beam (solid) is compared to the ratio of yields at  $\theta = 90^\circ, \phi = 0^\circ$  and  $90^\circ$  for a linearly polarized beam (dashed).

Previous measurements of photofission fragment angular distributions have been performed using an unpolarized beam for  $^{235}\text{U}$  [5],  $^{238}\text{U}$  and  $^{232}\text{Th}$  [3], and  $^{239}\text{Pu}$  [4] and fragment polarization asymmetries using a polarized beam were measured for  $^{238}\text{U}$  [11, 12] and  $^{232}\text{Th}$  [13]. Subscripts of  $f$  and  $n$  will be used to distinguish fragment quantities from neutron quantities. The results of Ref. [3] show that the value of  $A_f$  is large ( $\sim 1$  to 70) for photofission of  $^{238}\text{U}$  and  $^{232}\text{Th}$  at beam energies ranging from 5.0 to 7.0 MeV, while the measurements of Refs. [4, 5] show that over the same energy region the value of  $A_f$  is small ( $\sim -0.25$  to 0.3) for photofission of  $^{235}\text{U}$  and  $^{239}\text{Pu}$ . Using the measured fragment angular distribution in Ref. [3], the polarization asymmetry  $\Sigma_f$  is expected to be approximately 0.8 at  $\theta = 90^\circ$  for photofission of  $^{238}\text{U}$  at a beam energy of 6.0 MeV. This asymmetry implies that for every fragment emitted perpendicular to the plane of beam polarization, on average  $\sim 9$  fragments are expected to be emitted in the plane of beam polarization.

### C. Neutrons Generated from Fission

There are three general categories of neutrons that can be emitted during the fission process: early neutrons, prompt neutrons, and delayed neutrons. The differences in the

TABLE I. Average neutron yields from  $(n_{th}, f)$  of  $^{235}\text{U}$

Neutron Type	Average Neutron Yield $\bar{\nu}$	Fraction of Total Neutron Yield (%)
Early Neutrons	0.12 [16]	5
Prompt Neutrons	2.29 [16]	94
Delayed Neutrons	0.02 [17]	1

neutron angular distributions are attributed to the time during the fission process at which they are emitted. According to Ref. [14], early neutrons are emitted at any time between the initial absorption of the  $\gamma$  ray and the moment the fission fragments separate, prompt neutrons are emitted approximately  $10^{-18}$  s to  $10^{-15}$  s after fission, and delayed neutrons are emitted much later following fission. Early neutrons are assumed to be emitted with no preferred direction in the lab frame. Because the fission fragments reach 90% of their maximum kinetic energy within  $10^{-19}$  s [14], the prompt neutrons are emitted by almost fully accelerated fragments. The prompt neutrons are well-described by an evaporation process and are therefore assumed to be emitted with no preferred direction in the rest frame of the fragment [15]. Table I details the average neutron yields from each of these three categories for thermal neutron induced fission of  $^{235}\text{U}$  [16, 17].

The prompt neutrons make up the majority of the neutron yield and are emitted by almost fully accelerated fragments, therefore a correlation is expected between the photofission neutron angular distribution and the fragment angular distribution. This correlation has been confirmed by the measurement of Ref. [18] for near-threshold photofission of  $^{238}\text{U}$  and  $^{232}\text{Th}$  using an unpolarized beam. In this measurement, the neutron angular distribution was found to be anisotropic but significantly less anisotropic than the fragment angular distribution. This implies that if a linearly polarized beam is used to induce photofission, neutron polarization asymmetries may be measurable but should be smaller in magnitude than any fragment polarization asymmetries.

TABLE II. Masses and Enrichments of Actinide Targets

Target	Mass (g)	Enrichment (%)	Main Impurity
$^{235}\text{U}$	4.620	93.7	$^{238}\text{U}$ (6.3%)
$^{238}\text{U}$	6.884	99.1	-
$^{239}\text{Pu}$	3.808	94.0	$^{240}\text{Pu}$ (5.8%)
$^{232}\text{Th}$	17.36	99.9	-

## II. EXPERIMENT DESCRIPTION

### A. Beam and Target Information

The  $\gamma$ -ray beam for this experiment was generated at the High Intensity  $\gamma$ -ray Source (HI $\gamma$ S). The HI $\gamma$ S facility is a nearly-monoenergetic Compton  $\gamma$ -ray source with a wide energy range and switchable linear and circular polarizations. The facility and its use has been described in detail elsewhere [19–21], therefore only a short description is provided here. A nearly-monoenergetic, high-flux  $\gamma$ -ray beam is created by colliding a two-bunch electron beam in a storage ring with a high-power intra-cavity Free-Electron Laser (FEL) beam. For this experiment, the FEL wavelength was  $\sim 540$  nm and the electron beam energies were selected to produce  $\gamma$ -ray beams between 5.6 - 7.3 MeV, with an energy spread (FWHM) of  $\sim 3\%$ . The  $\gamma$ -ray beams were produced having either circular or linear polarizations. Because of the duty factor of the electron storage ring, the  $\gamma$ -ray beam is pulsed with a period of 179 ns. The temporal structure of the  $\gamma$ -ray beam made possible the use of a time-of-flight method to determine neutron energies. The absolute  $\gamma$ -ray intensity was measured using a set of precision Cu attenuators and a large NaI detector. The measured intensity, which ranged from  $3 \times 10^6 \gamma/s$  to  $7 \times 10^6 \gamma/s$ , was calibrated and monitored with an array of five plastic scintillating paddles as described in Ref. [22]. Table II gives the masses and enrichments of the four actinide targets used in the present work.

### B. Detector Array and Electronics

An array of eighteen detectors was used to identify neutrons generated from photofission. The active volume in each detector was filled with BC-501A liquid scintillator and was 12.7



FIG. 2. (Color online) A schematic of the half-meter flight-path detector array

cm in diameter and 5.1 cm thick. Twelve detectors were placed at  $\theta = 55^\circ, 90^\circ$ , and  $125^\circ$  and at  $\phi = 0^\circ, 90^\circ, 180^\circ$ , and  $270^\circ$ . Six detectors were placed at  $\theta = 72^\circ, 107^\circ$ , and  $142^\circ$  and at  $\phi = 0^\circ$  and  $90^\circ$ . The detector array is shown in Fig. 2. The target was positioned at the center of the array, and the flight path from the target to each detector was approximately 57 cm.

The electronic circuit used to process the detector signals was built using Mesytec MPD-4 modules [23]. This module used a detector signal as an input and returned separate signals containing pulse height (PH), pulse-shape discrimination (PSD), and a gate for each event that exceeded a threshold PSD value. The PSD value was used to discriminate against photon-like events. Digitization of the MPD-4 outputs was performed by analog-to-digital converters (ADCs) and the gates were used to measure the time-of-flight using time-to-digital converters (TDCs).

### C. Detector Calibration

Source runs were taken using an AmBe source to adjust the MPD-4 PSD threshold settings and effectively discriminate  $\gamma$  rays from neutrons.  $^{137}\text{Cs}$  source runs were also taken in order to set detector thresholds. Due to the finite resolution of the detector and multiple scattering effects [24], the 662 keV  $\gamma$  ray from  $^{137}\text{Cs}$  appears as a Compton edge having a midpoint PH of 517 keV electron equivalent. Software PH cuts are made relative to this leading edge in fractional increments, such as  $1/2 \times \text{Cs}$ . Because of its importance

in determining software PH thresholds, multiple  $^{137}\text{Cs}$  source runs were taken each day to monitor any potential gain drifts in the detectors. No gain drifts greater than a few percent were observed.

#### D. Data Collection

As an experimental confirmation of the time-of-flight method used in this experiment, data were taken using a  $\text{D}_2\text{O}$  target. Because the energy of the neutron emitted upon photodisintegration of a deuteron depends only on the beam energy and emission angle, an accurate energy calibration of the detectors was made possible by these data. Data were then taken using a circularly polarized beam for each actinide target to correct for instrumental asymmetries which could affect the measurement of  $\Sigma_n$ , the neutron polarization asymmetry as given in Eqn. 4. Because the prompt neutron spectrum should remain unchanged over the range of  $\gamma$ -ray beam energies (5.6-7.3 MeV), only one beam energy (7.0 MeV) was used to correct for instrumental asymmetries. Then, a linearly polarized beam was used at a variety of beam energies for the four actinide targets. Typical run times varied from one to four hours for each beam energy and target.

### III. DATA REDUCTION AND ANALYSIS

The first cut applied to the data was a software PH cut. This cut ranged from  $1/4 \times \text{Cs}$  to  $1/2 \times \text{Cs}$ , or neutrons of approximately 1.0 MeV to 1.5 MeV, depending on the detector voltage and amount of electronic noise in the detector. Higher thresholds were chosen for detectors that exhibited more electronic noise. Well-known cable delays were used to calibrate the TDCs and determine the appropriate conversion from TDC value into nanoseconds. A two-dimensional cut on the prompt neutrons was applied to the TDC vs PSD spectrum, as shown in Fig. 3. Also noticeable in this figure is a narrow  $\gamma$ -ray scattering peak appearing earlier in time than the neutrons. By measuring the distance from the target to the detector and using this  $\gamma$ -ray peak, the energy of the detected neutrons was determined from their time-of-flight. The monoenergetic neutrons from the  $\text{D}_2\text{O}$  measurement were then used to make slight adjustments to correct for the finite thickness of the active volume of the detectors. The energy resolution of the detector system is 100 keV for 2 MeV neutrons and 325 keV for

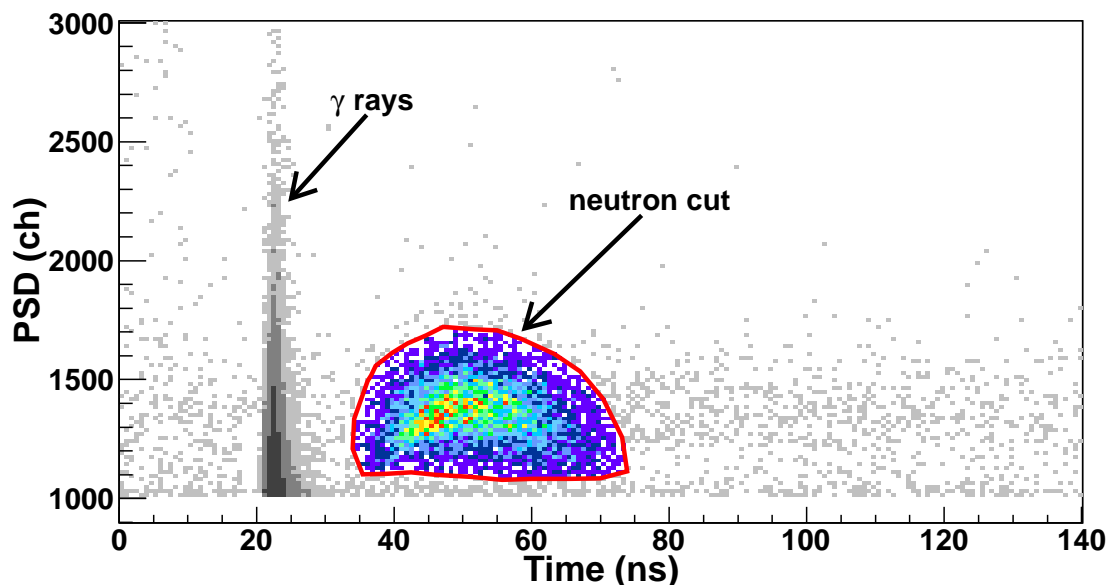


FIG. 3. (Color online) A typical two dimensional TDC vs PSD spectrum for prompt neutrons from photofission of  $^{232}\text{Th}$

6 MeV neutrons. Data uncorrelated with a  $\gamma$ -ray beam burst were measured using out-of-time cuts and used to subtract out background events. Sample neutron spectra are shown in Fig. 4. Even before correcting for instrumental asymmetries, significant polarization effects are apparent in the prompt neutrons from photofission of  $^{238}\text{U}$  and absent for  $^{235}\text{U}$ .

The neutron energy spectra were divided into 5 consecutive 1-MeV wide bins starting at  $E_n = 1.5$  MeV. The corrections to account for instrumental asymmetries for each neutron bin were calculated using the measurements with a circularly polarized beam. Because some detectors were placed at higher software PH thresholds to reduce noise, these corrections were significant and as large as 50% in some cases. If the detectors were all placed at the same software PH threshold, these corrections reduced to approximately 10%. These corrections were applied to the linearly polarized beam data, and corrected values of  $\Sigma_n$  were calculated.  $\Sigma_n$  was investigated as a function of  $\theta$ , the beam energy  $E_\gamma$ , and the neutron energy  $E_n$ .

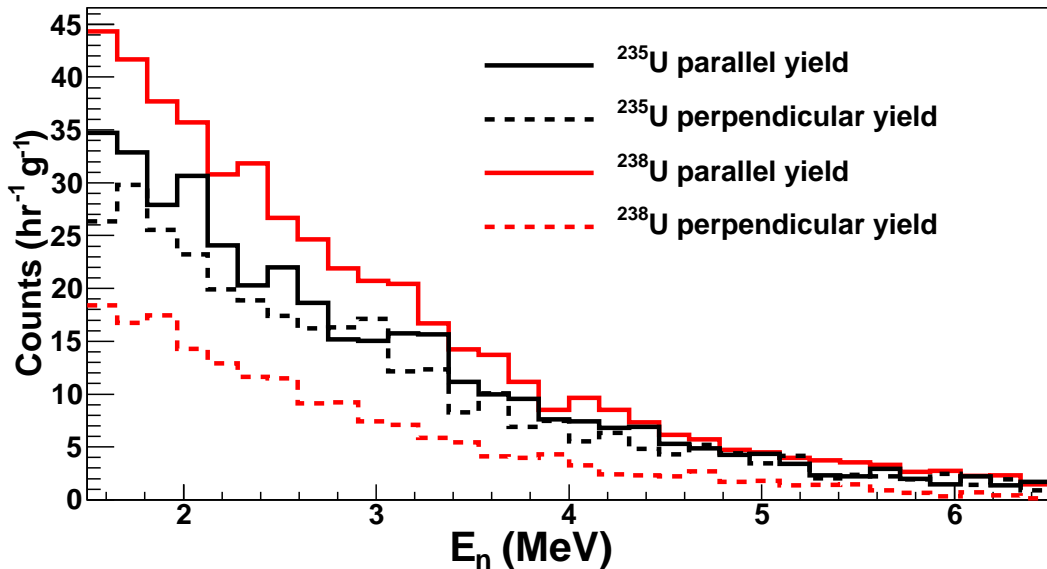


FIG. 4. (Color online) Prompt neutron spectra at  $\theta = 90^\circ$ , parallel and perpendicular to the plane of beam polarization are shown for photofission of  $^{235}\text{U}$  and  $^{238}\text{U}$ . The beams used here were 100% linearly polarized, had an average intensity of  $5 \times 10^6 \gamma/s$ , and had peak energies between 5.8 - 6.2 MeV. The detector thresholds were all set to  $1/4 \times \text{Cs}$ , or approximately  $E_n = 1.0$  MeV.

#### IV. RESULTS

The results of the measurement of  $\Sigma_n$  as a function of  $E_\gamma$  are shown in Fig. 5. Prompt neutrons from photofission of  $^{238}\text{U}$  and  $^{232}\text{Th}$  show large polarization effects especially for the lower beam energies studied. The differences between the results for  $^{238}\text{U}$  and  $^{232}\text{Th}$  are primarily due to the heights of their outer fission barriers, which are 6.2 MeV for  $^{232}\text{Th}$  and 5.7 MeV for  $^{238}\text{U}$  [25]. When the asymmetries are plotted as a function of the difference between the beam energy and the outer fission barrier height, the results for  $^{238}\text{U}$  and  $^{232}\text{Th}$  are almost identical. No significant polarization asymmetries are observed for prompt neutrons from photofission of  $^{235}\text{U}$ , and no asymmetries are observed for  $^{239}\text{Pu}$  except at low energies where small asymmetries less than unity were measured. The difference in spin between  $^{235}\text{U}$  ( $7/2$ ) and  $^{239}\text{Pu}$  ( $1/2$ ) is probably largely responsible for the observed differences in their measured asymmetries.

The dependence of  $\Sigma_n$  on  $E_n$  is shown in Fig. 6. For the even-even targets,  $\Sigma_n$  increases with increasing neutron energy. For the even-odd targets, no such correlation is observed.

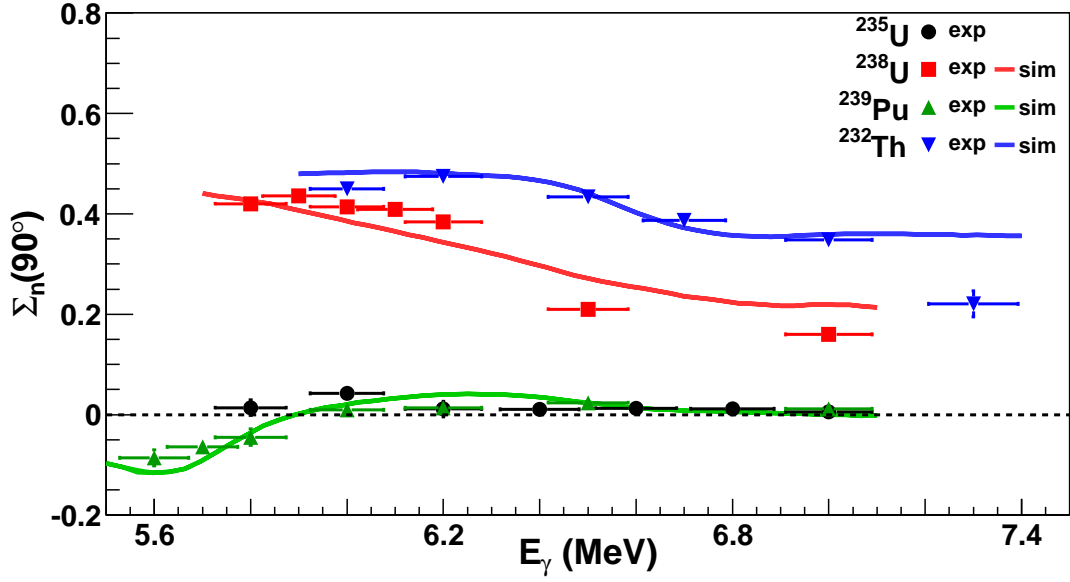


FIG. 5. (Color online) The measurement of  $\Sigma_n$  at  $\theta = 90^\circ$  for  $E_n > 1.5$  MeV is compared to the results of the simulation (full lines).

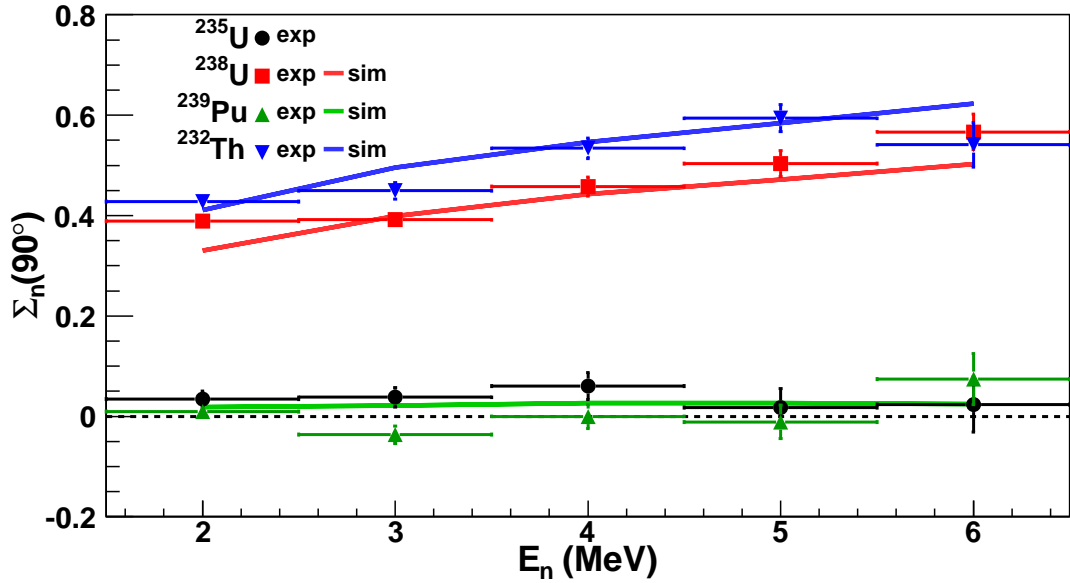


FIG. 6. (Color online) The measurement of  $\Sigma_n$  at  $\theta = 90^\circ$  for  $E_\gamma = 5.8 - 6.2$  MeV is compared to the results of the simulation (full lines).

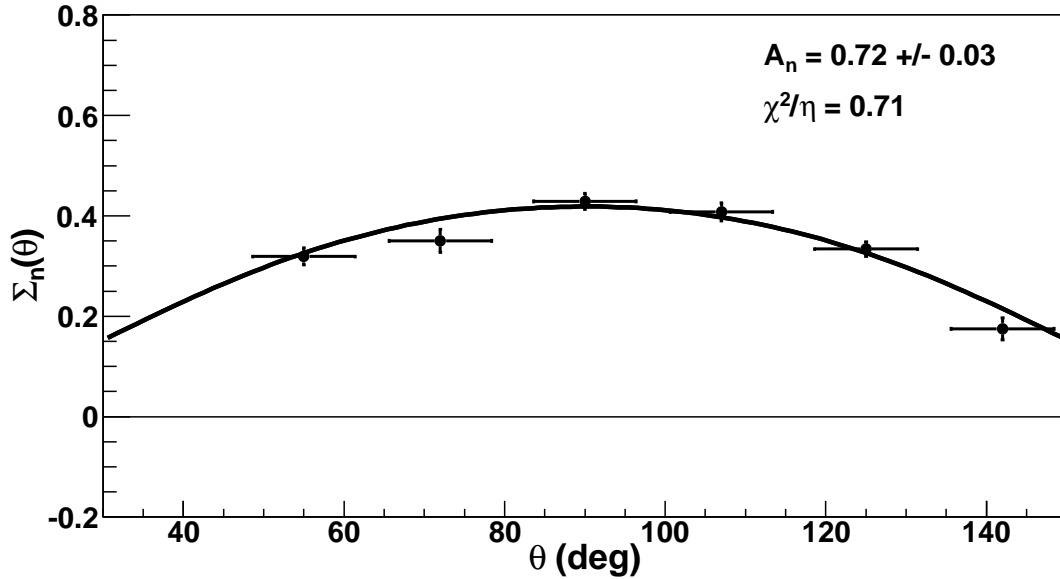


FIG. 7. The measurement of  $\Sigma_n$  as a function of  $\theta$ , for prompt neutrons from photofission of  $^{238}\text{U}$  using a 5.9 MeV linearly polarized beam, is compared to the result of a one parameter fit using Eqn. 5.

In addition to the measurements of  $\Sigma_n$  as a function of beam energy and neutron energy,  $\Sigma_n$  was investigated as a function of  $\theta$  to determine the coefficient  $A_n$  in Eqn. 5. A typical fit is shown in Fig. 7 and all of the resulting coefficients  $A_n$  are shown in Fig. 8 as a function of beam energy. Because the assumptions made in deriving Eqn. 5 are appropriate in this energy region, the average chi-squared per degree of freedom for these fits is about 0.8. The overall picture of prompt neutron polarization asymmetries remains qualitatively similar to Fig. 5.

## V. SIMULATION

A heuristic simulation of prompt neutron angular distributions has been developed to understand and interpret the differences in prompt neutron polarization asymmetries between even-even and even-odd targets. As an input, the simulation requires a known photofission fragment angular distribution. A simulation of  $^{235}\text{U}$  was not performed because the fragment angular distribution has been measured to be consistent with isotropy [5]. Previous measurements of photofission fragment angular distributions were performed using an unpolarized

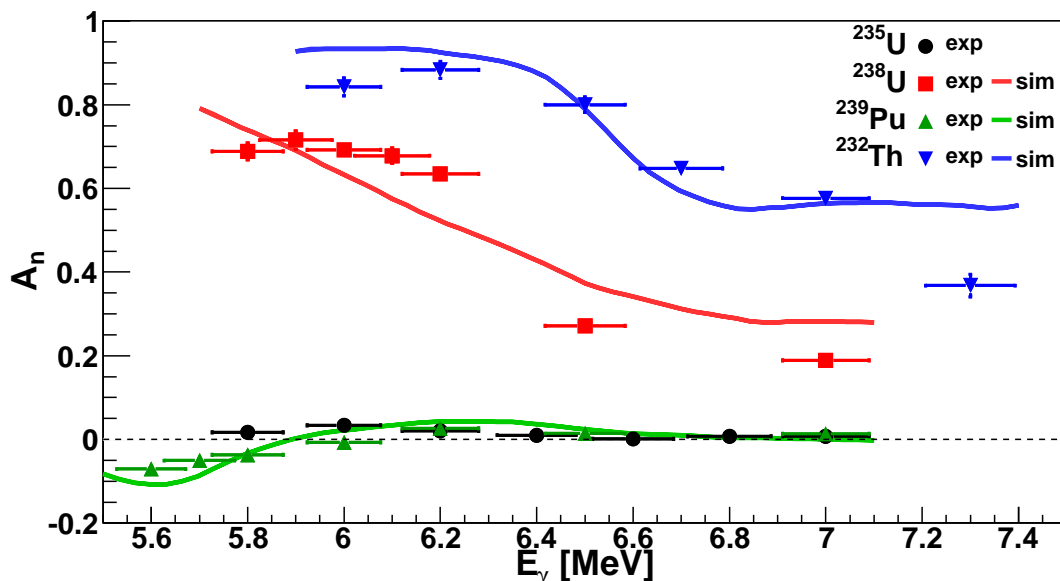


FIG. 8. (Color online) The results of a one parameter fit for  $A_n$  as a function of beam energy  $E_\gamma$  are compared to the results of the simulation (full lines).

bremsstrahlung beam for  $^{238}\text{U}$ ,  $^{239}\text{Pu}$ , and  $^{232}\text{Th}$  [3, 4], and anisotropic angular distributions were measured. In addition to reporting measured data, Refs. [3, 4] attempted to unfold the bremsstrahlung beam energy distribution from the raw data, and reconstructed photofission fragment angular distributions were provided as functions of photon energy. The reconstructed fragment angular distributions were assumed for the present simulations of prompt neutron polarization asymmetries from  $^{238}\text{U}$ ,  $^{239}\text{Pu}$ , and  $^{232}\text{Th}$ .

At the beginning of the simulation, the fragment angular distribution is used to predict the  $\phi$ -dependent fragment angular distribution under the assumption of E1 and E2 photofission only with no interference effects. Two fission fragments are generated according to this distribution at a particular beam energy. The masses of the fragments are randomly selected from the double-humped fragment mass distribution [26], and the total kinetic energy of the fragments is fixed to equal the measured average total kinetic energy of 170 MeV [9]. After the fragments' momentum vectors are calculated, each fragment is assumed to emit exactly one prompt neutron with no preferred direction in the rest frame of the fragment. It is well known that each fragment may emit more than one prompt neutron during fission [27]. In order to partially account for this potential bias in the simulation, the kinetic energy of the neutron in the rest frame of the fragment is not chosen from a single evaporation spectrum,

but instead from a spectrum which includes the effect of a second prompt neutron evaporated from a single fragment [15]. Then, the neutron is boosted into the lab frame and its lab momentum vector is calculated. The neutron is allowed to propagate in a straight line, and a hit is recorded if its path intersects a detector.

The results of the simulation, as shown by the lines in Figs. 5, 6, and 8, are in good quantitative agreement with the experimental measurement. The systematic differences between the even-even targets ( $^{238}\text{U}$  and  $^{232}\text{Th}$ ) and even-odd targets ( $^{239}\text{Pu}$ ) are accurately reproduced by the simulation. In addition, the simulation accurately predicts the trend of decreasing  $\Sigma_n$  with increasing beam energy. In the simulation, this trend occurs because the inferred fragment polarization asymmetries decrease with increasing beam energy for reasons outlined in Section I A. Another trend present in the results of the experiment and simulation is the increase of  $\Sigma_n$  with increasing neutron energy. This increase can be understood using the assumption that the neutrons are emitted by accelerated fragments. The neutrons that gain the most energy when boosted into the lab frame are those traveling in the same direction as the emitting fragment. Because the fragment polarization asymmetries are expected to be large, these higher energy neutrons have larger polarization asymmetries than lower energy neutrons, which were less likely to be traveling in the same direction as the fragment.

The good agreement between the results of the simulation and experimental measurement is apparent despite the simplifying assumptions made in the development of this heuristic model. For example, correlations exist between the average total kinetic energy of the fragments, the number of prompt neutrons emitted, and the mass division of the fragments [9]. A more advanced model is needed to simulate the effects of these additional complexities of the photofission reaction mechanism. However, the good agreement between the results of the experiment and the current simulation indicates that the essence of prompt neutron polarization asymmetries is captured in the simplified model.

## VI. CONCLUSIONS AND FUTURE WORK

The first measurements of prompt neutron polarization asymmetries have been performed at the HI $\gamma$ S facility. Prompt neutrons from photofission of  $^{238}\text{U}$  and  $^{232}\text{Th}$  at beam energies from 5.8 to 7.3 MeV exhibit large polarization asymmetries, while those from photofission

of  $^{235}\text{U}$  and  $^{239}\text{Pu}$  at these energies exhibit little or no polarization asymmetries. These asymmetries are well described by a simple model of photofission that assumes the prompt neutrons are emitted by fully accelerated fragments. The success of the simulation indicates that the prompt neutron polarization asymmetries are a result of expected fragment polarization asymmetries, which are inferred from measured unpolarized fragment angular distributions.

Future work will include extending the study to other actinides, including  $^{233}\text{U}$ ,  $^{240}\text{Pu}$ , and  $^{237}\text{Np}$ . Measurements of fragment polarization asymmetries will be performed for  $^{238}\text{U}$ . In addition to enhancing the experimental program, further improvements will be made to the photofission model in an attempt to better understand prompt neutron polarization asymmetries.

## VII. ACKNOWLEDGEMENTS

The authors wish to thank the HI $\gamma$ S staff for the beams produced during this experiment, and especially M. Emamian for his assistance in constructing and aligning the detector array.

This work was supported in-part by DNDO, Academic Research Initiative (ARI) Grant # 2010-DN-077-ARI46-02, ARI Grant # 2008-DN-077-ARI010, LLNL contract with DHS/DNDO HSHQDC-07-X-00213 P00015, DOE Grant # DE-FG02-97ER41033, and by the DOE Office of Science Graduate Fellowship Program (DOE SCGF), made possible in part by the American Recovery and Reinvestment Act of 2009, administered by ORISE-ORAU under contract # DE-AC05-06OR23100.

- 
- [1] E. J. Winhold, P. T. Demos, and I. Halpern, *Phys. Rev.* **87**, 1139 (1952).
  - [2] A. Bohr, ed., *Proc. U.N. Int. Conf. Peaceful Uses At. Energy*, 2 (New York, 1956).
  - [3] N. S. Rabotnov, G. N. Smirenkin, A. S. Soldatov, L. N. Usachev, S. P. Kapitza, and Yu. M. Tsipenyuk, *Sov. J. Nucl. Phys.* **11**, 285 (1970).
  - [4] A. S. Soldatov, Yu. M. Tsipenyuk, and G. N. Smirenkin, *Sov. J. Nucl. Phys.* **11**, 552 (1970).
  - [5] V. E. Zhuchko, Yu. B. Ostapenko, G. N. Smirenkin, A. S. Soldatov, and Yu. M. Tsipenyuk, *Sov. J. Nucl. Phys.* **27**, 746 (1978).

- [6] A. P. Baerg, R. M. Bartholomew, F. Brown, L. Katz, and S. B. Kowalski, *Can. J. Phys.* **37**, 1418 (1959).
- [7] L. P. Geraldo, *J. Phys. G: Nucl. Phys.* **12**, 1423 (1986).
- [8] J. J. Griffin, *Phys. Rev.* **116**, 107 (1959).
- [9] R. Vandenbosch and J. R. Huizenga, *Nuclear Fission* (Academic Press Inc., 1974).
- [10] L. W. Fagg and S. S. Hanna, *Rev. Mod. Phys.* **31**, 711 (1959).
- [11] S. G. Kadmsky, L. V. Titova, and O. S. Khmelevskaya, *Bulletin of the Russian Academy of Sciences: Physics* **73**, 831 (2009).
- [12] V. M. Khvastunov and V. V. Denyak, *Phys. At. Nucl.* **64**, 1269 (2001).
- [13] F. Steiper, T. Frommhold, W. Henkel, A. Jung, U. Kneissl, and R. Stock, *Nucl. Phys.* **A563**, 282 (1993).
- [14] C. Wagemans, ed., *The Nuclear Fission Process* (CRC Press, Inc., 1991).
- [15] J. S. Fraser, *Phys. Rev.* **88**, 536 (1952).
- [16] A. S. Vorobyev, O. A. Shcherbakov, Yu. S. Pleva, A. M. Gagarski, G. V. Val'ski, G. A. Petrov, V. I. Petrova, and T. A. Zavarukhina, *Nucl. Instrum. Meth.* **A598**, 795 (2009).
- [17] G. R. Keepin, T. F. Wimett, and R. K. Zeigler, *J. Nucl. Energy* **6**, 1 (1957).
- [18] S. Nair, D. B. Gayther, B. H. Patrick, and E. M. Bowey, *J. Phys. G: Nucl. Phys.* **3**, 965 (1977).
- [19] V. N. Litvinenko *et al.*, *Phys. Rev. Lett.* **78**, 4569 (1997).
- [20] H. R. Weller, M. W. Ahmed, H. Gao, W. Tornow, Y. Wu, M. Gai, and R. Miskimen, *Prog. Part. Nucl. Phys.* **62**, 257 (2009).
- [21] A. M. Bernstein, M. W. Ahmed, S. Stave, Y. Wu, and H. R. Weller, *Annu. Rev. Nucl. Part. Sci.* **59**, 115 (2009).
- [22] R. E. Pywell, O. Mavrighi, W. A. Wurtz, and R. Wilson, *Nucl. Instrum. Meth.* **A606**, 517 (2009).
- [23] A. Ruben *et al.*, *IEEE Nuclear Science Symposium Conference Record*, 681 (2007).
- [24] B. A. Perdue, Ph.D. thesis, Duke University (2010).
- [25] S. Bjornholm and J. E. Lynn, *Rev. Mod. Phys.* **52**, 725 (1980).
- [26] T. England and B. Rider, "Evaluation and compilation of fission yields," (1992), eNDF-349, LA-UR-94-3106, Extracted from ENDF.
- [27] J. T. Caldwell and E. J. Dowdy, *Nucl. Sci. Eng.* **56**, 179 (1975).